PHYSICAL REVIEW A **73**, 051802(R) (2006)

Self-organized bundle of lasing filaments in dense media

L. Guyon, F. Courvoisier, and V. Boutou
LASIM (UMR5579), Université Claude Bernard Lyon 1, 43 bd du 11 Novembre, 69622 Villeurbanne Cedex, France

R. Nuter, A. Vinçotte, S. Champeaux, and L. Bergé
Département de Physique Théorique et Appliquée, CEA-DAM/Ile de France, B.P. 12, 91680 Bruyères-le-Châtel, France

P. Glorieux
Laboratoire de Physique des Lasers, Atomes et Molécules, UMR 8523, Université de Lille I, Bâtiment P5-USTL 59655 Villeneuve d'Ascq Cedex, France

J.-P. Wolf
GAP, Université de Genève, 20 Rue de l'Ecole de Médecine, 1211 Genève 4, Switzerland
(Received 23 December 2005; published 8 May 2006)

The filamentation of powerful, ultrashort laser pulses in liquids is investigated. It is shown that the multiple filaments produced in ethanol can be modified into controllable, regular patterns by doping the medium with dyes at high concentrations. Experimental results are confirmed by three-dimensional numerical simulations. Pump-dump pulse experiments furthermore reveal that the stimulated emission from excited dye molecules in the bundle can be locked in phase and leads to bright interference patterns.

DOI: 10.1103/PhysRevA.73.051802 PACS number(s): 42.65.Tg, 52.38.Hb, 42.68.Ay

When ultrashort laser pulses propagate in transparent media, they create intense filaments, able to self-channel over long ranges. In the atmosphere, the self-channeling mechanism results from the interplay between Kerr focusing and multiphoton ionization [1]. At high enough powers, several filaments can be produced. They originate from modulational instability, which breaks up the beam into small-scale cells that convey a power close to a few critical powers for self-focusing. Multiple filaments first form from the initial beam defects, around which they are randomly nucleated, and further gather into a limited number of clusters, called "optical pillars." These clusters can then propagate over hundreds of meters, along which self-phase modulation considerably broadens the pulse spectrum [2]. Recently, Luo *et al.* [3] showed that the fluorescence from nitrogen molecules excited by a single filament, moreover, undergoes amplified spontaneous emission. Multifilamentation in air, nowadays, opens new perspectives in atmospheric diagnostics [4], such as multipollutant remote detection and bioaerosol identification using nonlinear terawatt lidars (light detection and ranging), long distance laser-induced breakdown analysis of solid targets, or megavolt-discharge triggering and guiding in view of lightning control.

Besides atmospheric propagation, the physics of femtosecond (fs) optical pulses in dense materials has become a challenging issue to understand the complex mechanisms that channel the light over shorter distances [5–9]. Recently, attempts have also been made to control the spatial position of filaments in water by shaping the spectral phase of an intense laser pulse [10]. Condensed media exhibit the property of amplifying some key parameters such as dispersion and plasma densities responsible for halting the wave collapse or maintaining the beam in focused state. In water, some experiments revealed that light filaments self-channel like an X-shaped wave while they reach an equilibrium between dispersion and a strong energy flux from the surrounding beam [9]. This apparent self-guiding is supported by important nonlinear losses such as multiphoton absorption. In liquids, the role of this nonlinear absorption in fs filaments can alternatively be investigated by adding dye fluorescent molecules, which, at low concentration, allows one to visualize the filamentation process [6].

In this work, we address two different issues using high concentrations of dye molecules in ethanol. We identify the role of multiphoton absorption losses in arranging filament patterns and prove the feasibility of inducing amplified stimulated emission from each filament. We show in a pump-dump configuration that: (a) A strong two-photon absorption (TPA) of dye molecules considerably reduces the number of filaments that organize within a latticelike arrangement, which is confirmed by three-dimensional (3D) numerical simulations. This leads to amplified spontaneous emission, as described by Prasad and co-workers from, e.g., coumarin [11]. (b) The fluorescence emitted from each filament is further locked in phase by a dump pulse superimposed with the pump, which allows the far-field observation of spectacular interference patterns, as self-organized arrays of "lasing" filaments.

In our experiment, the laser source is a Chirped-Pulse Amplifyer mode-locked Ti:sapphire oscillator, delivering 120–150 fs pulses at 810 nm with a 20 Hz repetition rate. A portion of this pump is set apart and focused in a 1-mm sapphire plate to generate a supercontinuum. To prepare the dump pulse, the 810-nm component is removed from the supercontinuum by a glass filter (BG 40) and the resulting beam is sent to an interferential filter centered at 530±5 nm, in order to calibrate its spectrum on the fluorescence band of the dye. The selected dye is coumarin 153, which has an absorption band ideally located for two-photon absorption with the 810-nm pump. The dump pulse energy does not

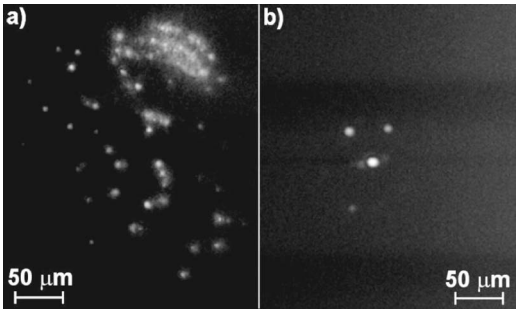

FIG. 1. Experimental fluence profiles at the cell exit after 1-cm-long propagation of an intense ($\sim 4\times10^{11}$ W/cm^2) pump pulse. (a) For pure ethanol, a multitude of filaments with $\sim 8-10$ μm in diameter are visible, whereas (b) with coumarin 153 ($C=4$ g/l), only a few filaments subsist in the bundle. In (b), the typical diameter of one filament is slightly less than 20 μm. The average distance between two neighboring filaments in the lattice is about 50–100 μm.

exceed a few tens of pJ. Both pump and dump pulses can then be recombined and carefully superimposed. They are slightly focused by a 1-m focal lens in order to illuminate a flow cell containing either pure or dye-doped ethanol. The incident pump pulse intensity at the cell entrance is around 4×10^{11} W/cm^2. Through the sample, the pump pulse not only develops filaments, but also induces two-photon excitation of dye molecules. To change the filamentation pattern, the spatial profile of the pump pulse can be modified with an iris placed a few centimeters before the entrance cell window. A charge-coupled device (CCD) camera is used to image the laser intensity of the pump on the iris and at the exit of the 1-cm-long cell.

We first examined the effect of high concentrations of coumarin up to 4 g/l on the generation of filaments in different beam geometries involving no dump pulse. The iris diameter was about 1 mm. On Fig. 1(a), a myriad of filaments emerges from the cell exit for pure ethanol. The diameter of each filament does not exceed a few microns, typically $8-10$ μm. In contrast, Fig. 1(b) shows the filamentation pattern created after adding coumarin with concentration $C=4$ g/l. In this configuration, the two-photon absorption kills most of the filaments. The size of the surviving light spots, although still of several microns, appears slightly enlarged to about $15-20$ μm. The distance between two adjacent filaments is about $50-100$ μm, designing a kind of lattice. These observations are consistent with previous ones [6], exploiting nonlinear losses to monitor multifilamentation in liquids.

In order to emphasize the role of dye absorption in softening filamentation, we performed numerical calculations based on a nonlinear Schrödinger (NLS) equation for the electric field envelope, $\mathcal{E}$, coupled to a Drude model for the plasma density, ρ. These equations can already be found in Refs. [1,12]. In the present context, they are integrated in full (3+1)-dimensional geometry, assuming weak contributions from space-time focusing and self-steepening for full width at half maximum (FWHM) pulse durations as large as 120 fs. The central wave number is defined by $k=n_0k_0$ with $k_0=2\pi/\lambda_0=\omega_0/c$, $\lambda_0=810$ nm, and $n_0=1.36$ for ethanol. Group-velocity dispersion (GVD) has the coefficient $k''\simeq 403$ fs^2/cm [13]. We consider an instantaneous Kerr response with basic index $n_2=2.6\times10^{-16}$ cm^2/W for pure ethanol [14]. When the dye is added, even at weak densities, this coefficient may change significantly. Recent studies indeed reported important changes in the nonlinear refractive index [15], capable of increasing by one to two decades. In the absence of precise measurements of n_2 for dilute solutions, we shall opt for $n_2^{\mathrm{dye}}=2.6\times10^{-15}$ cm^2/W. The critical power for self-focusing, defined as $P_{\mathrm{cr}}=\lambda_0^2/2\pi n_0 n_2$, is then $P_{\mathrm{cr}}\simeq 3$ MW for pure ethanol, but $P_{\mathrm{cr}}\simeq 0.3$ MW when the dye is dissolved in the sample. Plasma gain and losses apply to ionization of ethanol molecules mainly. Electron transitions to the conduction band take place with the gap potential $U_i=8.4$ eV, yielding six photon transitions [16] at 810 nm with multiphoton cross section $\sigma_{K=6}=5.63\times10^{-69}$ s^{-1} cm^{12}/W^6 [17], for the neutral density $\rho_{\mathrm{nt}}=1.03\times10^{22}$ cm^{-3}, critical plasma density $\rho_c=1.7\times10^{21}$ cm^{-3}, and inverse bremstrahlung cross section $\sigma\simeq 1.22\times10^{-17}$ cm^2. Coumarin 153 mainly contributes to lower the beam intensity through a TPA additional term introduced into the NLS equation such as $d_z I=-\sigma_{\mathrm{abs}}^{(n=2)}\rho_{\mathrm{abs}}I^2$ [18]. The coumarin density ρ_{abs} is 7.8×10^{18} cm^{-3} for $C=4$ g/l and the TPA cross section is $\sigma_{\mathrm{abs}}^{(2)}=6.76\times10^{-31}$ cm^4/W [19]. The model also accounts for avalanche ionization and electron recombination ($\tau_r=450$ ps [20]).

To simulate the previous results, we consider initial laser fields, for which input powers, peak intensities, and beam waist are those of the experimental values. The beam cut by an iris is modeled by a super-Gaussian spatial shape completed by a temporal Gaussian profile;

$$\mathcal{E}(x,y,t,z=0)=\sqrt{\frac{2^{1/N}P_{\mathrm{in}}}{\Gamma\left(1+\frac{1}{N}\right)\pi w_0^2}}\times e^{-((x^2+y^2)/w_0^2)^N-t^2/t_p^2}, \tag{1}$$

which we perturb by a 15% amplitude random noise. Here, $\Gamma(x)$ is the usual Euler function, $N=10$, $w_0=0.5$ mm, and $t_p=102$ fs. The peak power $P_{\mathrm{in}}\simeq 2.8$ GW together with the input peak intensity $I_0^{\max}=4\times10^{11}$ W/cm^2 are equal to their experimental counterparts.

Figures 2(a,b) display the fluence profiles in the (x,y) plane, computed at the cell exit for the initial condition (1). These patterns are in qualitative agreement with Fig. 1. For pure ethanol, the cut beam decays into a high number of filaments with a diameter close to $8-10$ μm. More precisely, it first produces two ring structures, originating from the sharp edges of the diaphragm. The intensity of these rings is then amplified by the Kerr effect, which induces a growth of their gradient and breaks them up into light spots by azimuthal modulational instability. This gives rise to small-scale filaments that develop more and more towards the center of the sample as the beam propagates. This observation agrees with Ref. [21], where it was shown that the filamentation process occurs mainly in spatial area with strong field gradients. Figure 2(b) exhibits the fluence profiles calculated at the cell exit for a coumarin/ethanol solution. We observe that

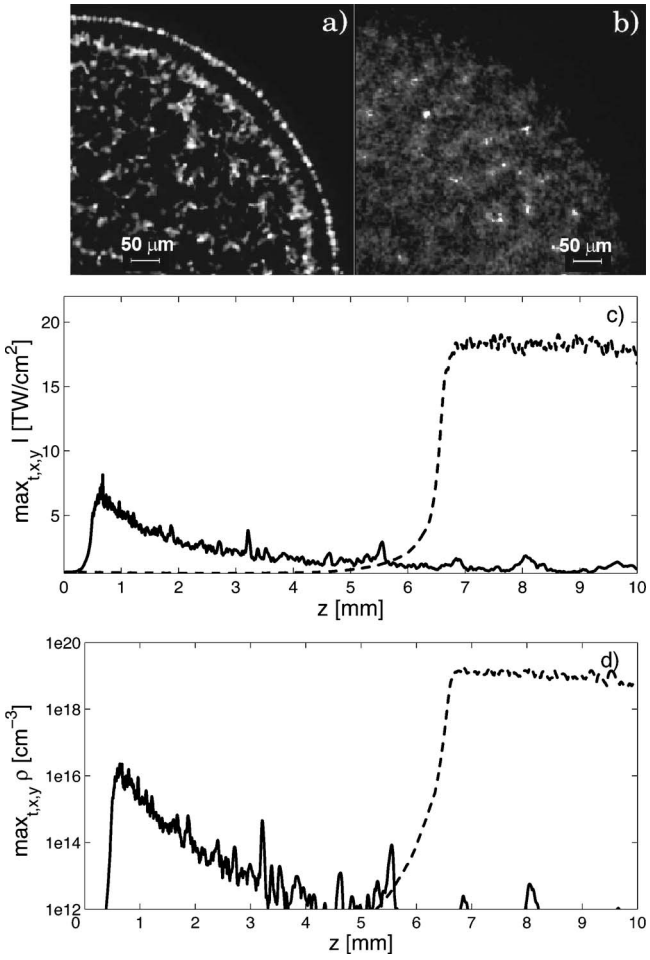

FIG. 2. Calculated fluence profiles at the cell exit for (a) pure ethanol and (b) ethanol + coumarin. Calculations and experiments (Fig. 1) are in good agreement, emphasizing spot average diameters of 8–10 μm in pure ethanol and doubled otherwise, with separation distances of ~50–100 μm. (c) Peak intensity and (d) electron density for pure (dashed curves) and dyed (solid curves) ethanol along the 1-cm-long cell.

the dye turns off some filament sites, decreasing thereby the spot number. In accordance with the experimental measurements, Fig. 2(b) also displays small-scale filaments with an average diameter larger than in pure ethanol. This is directly linked to the nonlinear damping action of coumarin, which contributes to stop the beam collapse at lower intensity values. The interfilament distance of ~50–100 μm is retrieved.

Figures 2(c) and 2(d) show the peak (maximum over x,y,t) intensities and related electron densities for the whole multifilamented beams involving coumarin or not along the z axis. The "ripples" affecting these curves signify that at some distances z the intensity of one filament suddenly takes over that of its most intense neighbors. For pure ethanol, the field self-focuses in intensity up to 18 TW/cm^2 until the nonlinear focus $z_c \simeq 7$ mm. The beam collapse is stopped by the generation of plasma reaching a peak density around 10^{19} cm^{-3}. The pulse then self-channels over 3 mm through the dynamic balance between Kerr self-focusing and the defocusing plasma. This process is accompanied by weak energy loss (6%) caused by ionization of the neutral species. When

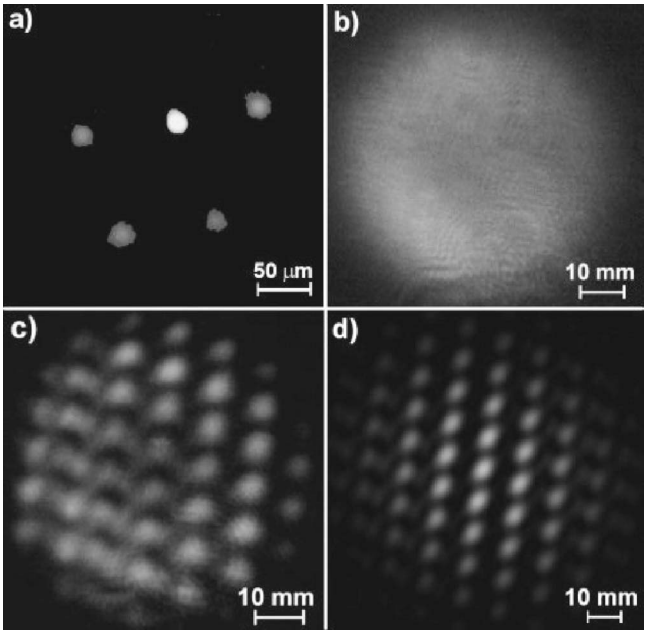

FIG. 3. Complete pump-dump lasing experiment. (a) Filamentary lattice at the cell exit. (b) Incoherent spontaneous emission in the far field. (c) Far-field interference pattern in presence of the dump pulse which stimulates and locks in phase the emission of each filament. (d) Fourier transform of the filament bundle displayed in (a).

the beam propagates in the dilute dyed solution, the coumarin TPA, which is an intensity dependent mechanism, absorbs pulse energy from the early stages, but becomes fully efficient in the filamentation domain where the beam attains high intensities. As a result, it enhances the overall energy loss to ~80% over 1 cm (not shown here) and smoothes spatial distortions as it decreases the filamentation growth rate [18]. We observe a backward motion of z_c to 0.8 mm, mainly due to the higher value of n_2. From this distance, the peak intensity only reaches 8 TW/cm^2 and the electron plasma hardly attains the density 10^{16} cm^{-3}, before it rapidly falls down to levels lower than 10^{14} cm^{-3}. In this case, Kerr self-focusing mainly competes with coumarin TPA that becomes the dominant damping mechanism. Compared with nonlinear losses caused by ethanol ionization (six-photon transitions), TPA not only arrests self-focusing, but it also prevents the pulse from self-channeling by keeping its intensity clamped at constant value. So, no dynamic balance takes place, unlike propagation in pure ethanol.

The agreement between experiments and calculations is fairly good. In the absence of coumarin, the propagation of the pump pulse through 1 cm of ethanol produces many narrow filaments. In contrast, with coumarin the filaments strongly decrease in number and their size is broader. The calculation also exhibits that the filament intensity is weaker than for pure ethanol. However, because of the self-focusing, with a mean intensity of $\langle I \rangle \sim 3$ TW/cm^2 at $C=4$ g/l, the density of two-photon excited coumarin molecules attains $\rho_{\mathrm{exc}} = \sqrt{\pi}\sigma^{(2)}_{\mathrm{abs}}\rho_{\mathrm{abs}}\langle I \rangle^2 T/(4\hbar\omega_0) \simeq 9 \times 10^{17}$ cm^{-3} using the typical filament duration $T \sim t_p/10$ [1]. The amount of excited molecules thus appears high enough to trigger amplified stimulated emission and to measure it.

In the second series of experiments, a dump pulse at 530 nm is superimposed to the pump. The purpose is to undertake coherent amplified stimulated emission in the filament bundle. As reported by Cook *et al.* [22], white light filaments emerge in phase in liquids due to the coherence property of the continuum induced by the optical Kerr effect. In contrast, we do not exploit this Kerr-induced coherence. Here, the addition of coumarin does not only allow control of the filamentation pattern, but it also provides each filamentary site with a reservoir of excited dye molecules, ready to fluoresce, to achieve a population inversion. The dump pulse then triggers in-phase stimulated emission from each filament, which leads to an interference pattern, as shown in Fig. 3. Figure 3(a) exhibits the intensity of the pump at the output of the cell filled with an ethanol/coumarin solution (4 g/l). A set of five self-arranged filaments is visible. Far-field pictures of the coumarin emission are then taken in the forward direction, about 2 m after the cell. If the dump pulse is set to zero, we observe a uniform incoherent emission of low intensity [see Fig. 3(b)], whereas if the dump pulse is switched on, a bright interference pattern is visible in Fig. 3(c) which arises from the stimulated emission in each filament. The lasing intensity can be a hundred times higher than the amplified spontaneous emission intensity measured without the dump pulse. In Fig. 3(d), we calculated the Fourier transform of the filament bundle (FTFB) corresponding to Fig. 3(a). The intensity of the brightest filament in Fig. 3(a) was saturated and thus corrected to retrieve the FT image. The agreement between the far-field interference pattern [Fig. 3(c)] and the FTFB is close to excellent. The smallest distance between two bright interference spots (i.e., about 10 mm) in Figs. 3(c) and 3(d) is directly related to the distance between two adjacent filaments (i.e., about 50–100 μm) in Fig. 3(a). The extension of the interference pattern depends on the brightness equilibrium of filaments in the bundle. Note that, at least in the available pump-dump delay range of 0–150 ps, no difference in the observed interference patterns was noticeable. Other configurations delivered by the spatial profiles of the input pump were also observed, leading in particular to pure flowerlike patterns with perfect hexagonal symmetry. Such configurations will be discussed in a forthcoming paper.

In summary, we have investigated the multiple filamentation in dye-doped ethanol promoting strong two-photon absorption losses in ultrafast pump-dump experiments. A (3+1)-dimensional code was used to reproduce and understand the experimental patterns. Inside the bundle, sparse filaments organize in lattice, unlike their random nucleation in pure ethanol. Besides, the dump process coherently locks in phase the amplified stimulated emission in each filament and leads to the observation of interference patterns in the far field. "Lasing" filaments open promising trends in the possibility of amplifying stimulated emission in condensed media over short propagation distances.

The authors aknowledge J. Moloney and M. Kolesik for fruitful discussions.

[1] S. Skupin *et al.*, Phys. Rev. E **70**, 046602 (2004), and references therein.
[2] M. Rodriguez *et al.*, Phys. Rev. E **69**, 036607 (2004); J. Yu *et al.*, Opt. Lett. **26**, 533 (2001).
[3] Q. Luo, W. Liu, and S. L. Chin, Appl. Phys. B **76**, 337 (2003).
[4] J. Kasparian *et al.*, Science **301**, 61 (2003); see also www.teramobile.org.
[5] W. Liu, S. L. Chin, O. Kosareva, I. S. Golubtsov, and V. P. Kandidov, Opt. Commun. **225**, 193 (2003).
[6] H. Schroeder and S. L. Chin, Opt. Commun. **234**, 399 (2004); J. Liu *et al.*, Opt. Express **13**, 10248 (2005).
[7] H. Ward and L. Bergé, Phys. Rev. Lett. **90**, 053901 (2003).
[8] M. Kolesik, E. M. Wright, and J. V. Moloney, Phys. Rev. Lett. **92**, 253901 (2004).
[9] A. Dubietis, E. Gaizauskas, G. Tamosauskas, and P. Di Trapani, Phys. Rev. Lett. **92**, 253903 (2004).
[10] G. Heck, J. Sloss, and R. J. Levis, Opt. Commun. **259**, 216 (2006).
[11] G. S. He, R. Signorini, and P. N. Prasad, Appl. Opt. **37**, 5720 (1998).
[12] L. Bergé and S. Skupin, Phys. Rev. E **71**, 065601(R) (2005).
[13] J. Rheims, J. Köser, and T. Wriedt, Meas. Sci. Technol. **8**, 601 (1997).
[14] Q. H. Gong, J. L. Li, T. Q. Zhang, and H. Yang, Chin. Phys. Lett. **15**, 30 (1998).
[15] S. Yamakawa, K. Hamashima, T. Kinoshita, and K. Sasaki, Appl. Phys. Lett. **72**, 1562 (1998); R. A. Ganeev *et al.*, J. Opt. A, Pure Appl. Opt. **6**, 282 (2004).
[16] J. M. Jung and H. Gress, Chem. Phys. Lett. **359**, 153 (2002); J. M. Jung, Chem. Phys. Lett. **366**, 67 (2002).
[17] L. V. Keldysh, Sov. Phys. JETP **20**, 1307 (1965).
[18] P. Donnat *et al.*, Opt. Lett. **17**, 331 (1992).
[19] A. Fischer, C. Cremer, and E. H. K. Stelzer, Appl. Opt. **34**, 1989 (1995); B. Kovac and I. Novak, Spectrochim. Acta, Part A **58**, 1483 (2002).
[20] Q. Feng *et al.*, IEEE J. Quantum Electron. **33**, 127 (1997).
[21] L. Bergé, C. Gouédard, J. Schjødt-Eriksen, and H. Ward, Phys. Scr. **176**, 181 (2003).
[22] K. Cook *et al.*, Appl. Phys. Lett. **83**, 3861 (2003).